IASS 2018 BOSTON, JULY 16-20
CREATIVITY IN STRUCTURAL DESIGN

Proceedings of the IASS Annual Symposium 2018
Creativity in Structural Design
July 16-20, 2018, MIT, Boston, USA
Caitlin Mueller, Sigrid Adriaenssens (eds.)

Structural Behavior of a Cast-in-Place Funicular Polyhedral Concrete: Applied 3D Graphic Statics

Mohammad BOLHASSANI*, Ali TABATABAEI GHOMI, Andrei NEJUR, Mustafa OMER FURKAN[a], Ivan BARTOLI[a], Masoud AKBARZADEH

* Polyhedral Structures Laboratory, School of Design, University of Pennsylvania,
Pennovation Center, 3401 Grays Ferry Ave. Philadelphia, PA, 19146
Email: mb3238@upenn.edu

[a] Department of Civil, Architectural and Environmental Engineering, Drexel University,
Philadelphia, PA, 19104

Abstract

Although geometry-based structural design methods like 3D Graphic Statics (3DGS) allow for exploring a variety of spatial funicular geometry and their force equilibria. However, the material properties are not involved in the geometric form finding and there is no experimental data on the actual mechanical behavior of such systems. This paper will explore the structural performance of a funicular polyhedral geometry using experimental testing. The geometry of the physical prototype for the presented study is designed using 3DGS method. The specimen is constructed as a cast-in-place concrete structure, and the geometry of the sample is comparable to the standard concrete cylindrical test. High-performance, self-consolidating concrete is used for casting. Experimental results validated the 3DGS force distribution in the structure and showed that the magnitude of internal force in the members of the sample can be accurately predicted by 3DGS as long as the ultimate strength of the specimen is known.

Keywords: Funicular polyhedral structure, cast-in-place spatial concrete, structural behavior, 3D graphic statics

1. Introduction

Designing funicular structural forms using conventional graphic statics methods (Maxwell [1], and Rankine [2]) is a popular method to design efficient structures (Guastavino [3], and Ochsendorf [4]). However, these methods are all limited to 2D/2.5D. On the other hand in 3D, using sequential topology, shape and size optimization in form-finding and analysis procedure have been frequently used in the literature to design efficient light-weight structures. For instance, the very same method has been recently used for constructing an ultra-thin, concrete vaulted floor system by López López et al. [5], and Liew et al. [6]. In 2016, Akbarzadeh [7] developed an equivalent method of 2DGS in 3D. This new method (3DGS) allows for exploring a variety of spatial funicular geometry, however, the material properties are not involved in the geometric form finding and there is no experimental data on the actual mechanical behavior of such systems. For instance, Hedracrete is a prefabricated, concrete polyhedral structure and the first manifestation of 3DGS methods (Bolhassani et al. [8]). The form is a self-supporting, funicular polyhedral geometry with combined compression and tension members that pushes the boundaries of using concrete in the construction of spatial structures. MycoTree is another example of applied 3DGS. It is a compression-only spatial structure made of load-bearing mycelium and bamboo (Heisel et al. [9]). Although there are several prototypes designed and constructed by 3DGS as mentioned, this method has not been experimentally verified. Therefore, presented research is the first attempt to validate the results of 3DGS experimentally. The main objective of the paper is to experimentally investigate the structural behavior of a cast-in-place funicular polyhedral concrete structure (e.g., internal force of members, failure mode, and ultimate strength) designed by 3DGS.

2. Fabrication of the Specimen

Form-finding, geometry: A parametric bar-node model is developed using 3DGS methods allowing the change in the supports positions, magnitude, angle and distribution of applied forces, and the overall proportion while preserving the reciprocal relationship between form and force diagrams (Fig. 1). Standard concrete compressive test cylinder's proportion (1d to 2h) is used in this model. Fabrication and feasibility parameters determined the minimum and maximum radius of the members, and it changes between 18mm (0.7in) and 36mm (1.4in). The ratio of radius of each member to other members is equal to the ratio of magnitude of the force inside that member to other members. This means the distribution of volume is based on the distribution of forces in 3DGS model. The mold is printed as discrete elements and glued together (see Fig. 2a and b). Then concrete is poured and finally after it sets the mold is removed (Fig. 2c and d).

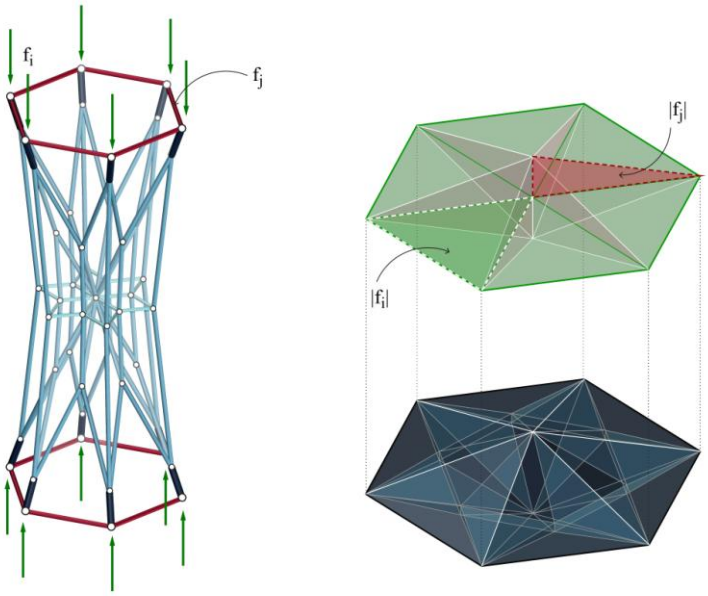

Figure 1: Form and force diagrams

Concrete mixture: Due to the small size of members and the complex geometry of the specimen, self-consolidating concrete is used for casting. Additionally, in order to check the accuracy of 3DGS prediction, relatively highly stiff linear-elastic material should be used to fabricate the model. This is mainly due to the linear-elastic modeling behind the 3DGS design. Therefore, a high strength concrete mix design is chosen in this research.

Commercial Portland cement type I (QUIKRETE®) along with all-purpose sand are used in this study. Pozzolanic material, gray silica fume (Sikacrete®-950 DP) with average particle size of 900nm (3.4E-5in), is used for achieving a higher strength and higher modulus of elasticity. High range water reducing admixture polycarboxylic polymer based super plasticizer (Sika® ViscoCrete®-2100) produced by Sika Corporation is also used for the mixture. Monofilament Polypropylene concrete micro fiber (SikaFiber® HP) with the maximum 12mm (0.5in) length is used mostly to control the shrinkage of concrete.

First, sand and fiber are mixed, then the measured silica fume and cement are added into the initial mix. Next, super plasticizer and water are measured and mixed separately and then the final liquid is added to the dried mix of sand, fiber, cement, and micro silica. Mixture is blended for 5 minutes with a rate of 80rpm. Afterwards, it is blended for 2 extra minutes with a rate of 120rpm for the second round. Finally, the specimens are casted in the prepared mold. In addition, one 304mm x 152mm (12in x 6in) cylinder following ASTM C39 [10] and one 50mm x 50mm (2in x 2in) cube are poured as well for the compressive strength test. All the specimens are cured in the standard experimental condition at 20±2°C (68±3.6°F) in a water tank for 28 days.

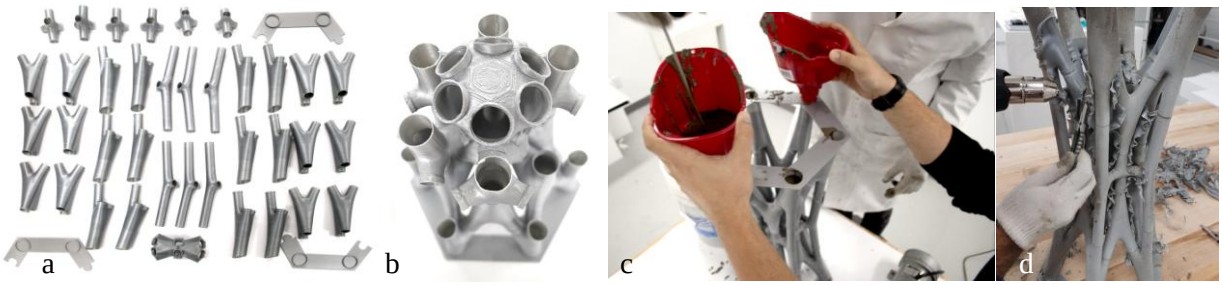

Figure 2: Construction of the specimen; (a) mold parts; (b) assembly; (c) casting concrete; (d) removing the mold

3. Test Setup and Instrumentation

Tinius-Olsen electromatic universal test machine (Model 398 display & CMM 496 controller) with the nominal capacity of 534kN (120kips) is used to test the specimen. This machine can measure the load and displacement within the range of ±1%. The rate of test was fixed at 0.2 mm/min (0.01in/min). To confine the top and bottom parts from any lateral movements two 12mm (0.5in) thick steel plates with the hexagonal 12mm by 12mm (0.5in x 0.5in) steel bars welded all across are used as caps, see Figure 3a. Caps are fabricated approximately 6mm (0.25in) larger than the size of the actual specimen and gypsum is spread on the steel plate to fill the gap and also level the caps in case the surface of the specimen is not sufficiently smooth or level. All strain gages are installed using super glue on the surface of specimen. After installing the strain gages the specimen was painted white to make any cracks visible and track them progressively during the test (Fig. 3c).

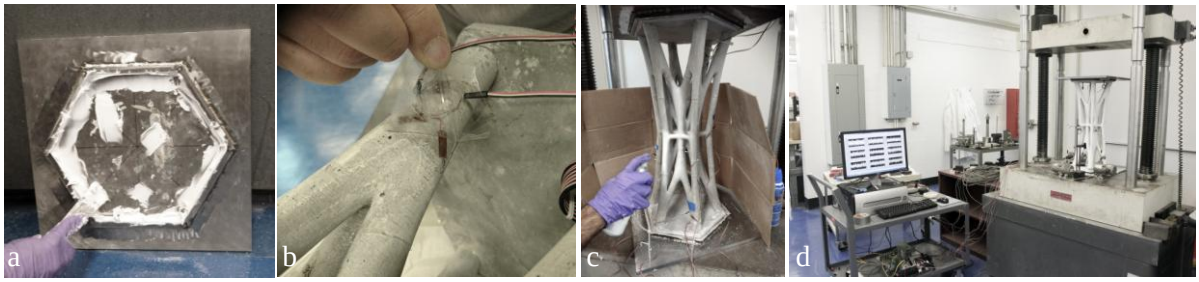

Figure 3: Test setup; (a) cap, (b) strain gage installation, (c) spraying the specimen, (d) test setup

As previously mentioned the universal test machine has an accurate displacement gage and load cell. However, displacement reading from the machine can be different from the actual deformation of the specimen due to flexibility of the testing frame and also calibration error. Additionally, the displacement value is the average reading of the motion at the threaded rods which does not provide any data regarding the asymmetric loading. Therefore, two more string potentiometers (SP1 and SP2) were installed on both sides of the specimen to measure the actual deformation of specimen and record any potential asymmetric deformation of the specimen during the test. Another potentiometer (SP3) is installed at the mid height of the specimen to measure lateral deformation.

Due to symmetrical geometry of the specimen, eight strain gages are mounted at different locations to measure strain as depicted in Figure 4. Four of them are installed at the bottom part (B1-B4) and the other four at the top cross side (T1-T4). B1, B2 and T1, T2 are installed as a 90-degree rosette for measuring shear strain. Other strain gages are simply measuring the axial compression strain of the designated member during the test.

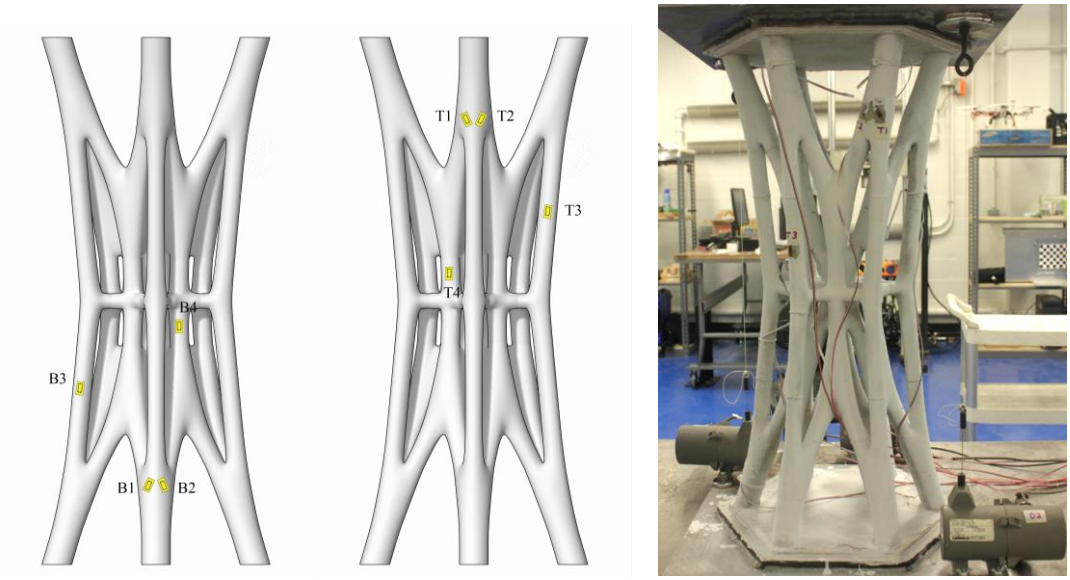

Figure 4: Strain gage locations

4. Experimental Results

The average 28 days compressive strength of concrete is 46MPa (6,630psi) (see Table 1). The secant modulus of elasticity specified by ACI Committee 363–10 is used to calculate the modulus of elasticity of the concrete [11].

Table 1: Compressive strength of concrete at 28 days

Name	Load kN (kips)	Area cm^2 (in^2)	f'c MPa (ksi)	E GPa (ksi)
Cylinder	359 (81)	81.3 (12.6)	44.2 (6.4)	29.0 (4,204)
Cube	122 (27)	26.0 (4.0)	47.2 (6.8)	29.7 (4,308)
Average	-	-	45.7 (6.6)	29.3 (4,256)

Comparison between the potentiometer measurements showed a slight difference between left and right side of the specimen. As can be drawn from Fig. 5a, 0.5 mm (0.02in) is recorded as the maximum gap between the two potentiometers. This means the top loading plate was not completely level during the test and experienced 0.08% slope. This causes the specimen to slightly undergo non-uniform compression. Strains of members are plotted versus the displacement of the loading plates in Fig 5b. The behavior of the specimen can be divided into three zones in terms of deflection:

Zone A; (0 to 1.5mm): In this phase the structure has adjusting itself under the load. As it can be seen from Fig. 5b most of the members do not experience any strain up to this point. Additionally, some of the members are experiencing tensile stress due to unbalanced loading in this zone. This unbalanced loading condition is mainly due to the unlevel steel loading plate that causes some tensile cracks in the members as shown in Fig. 6a. However, the specimen is still adjusting itself under the load and this crack does not affect the overall behavior of the structure.

Zone B; (1.5 to 3mm): The specimen is fully engaged with the testing machine and any imposed displacement transfers to all members. Strains are proportionally related to applied load and specimen is loaded to 217kN (49kips) at the end of this stage (first peak). At point 2.9mm (0.115in) one of the members fails causing a sudden increase in strain in all other members due to rapid redistribution of applied load. The failed member is shown in Fig. 6b. Strain gage B3 which was mounted on the failed member and stopped recording data at this stage. Additionally, the jump in the measured strain, after

the local failure, in all of designated members is the same which shows that the load distributed evenly between remained members.

Zone C; (3 to 3.3mm): The specimen gains more load after losing one of its long columns by almost same rate as in zone B until it reaches its ultimate strength (236kN (53kips), second peak). Due to efficiency of design and high strength concrete all the members reached their maximum strength simultaneously and instead of local failure in one member the specimen exploded under the final load (Figure 6c shows the failure mode). SP3 reading shows almost zero deformation during the test in the lateral direction. This means the specimen did not show any global buckling tendency or geometrical instability and instead behaved completely in compression.

(a) load-deformation

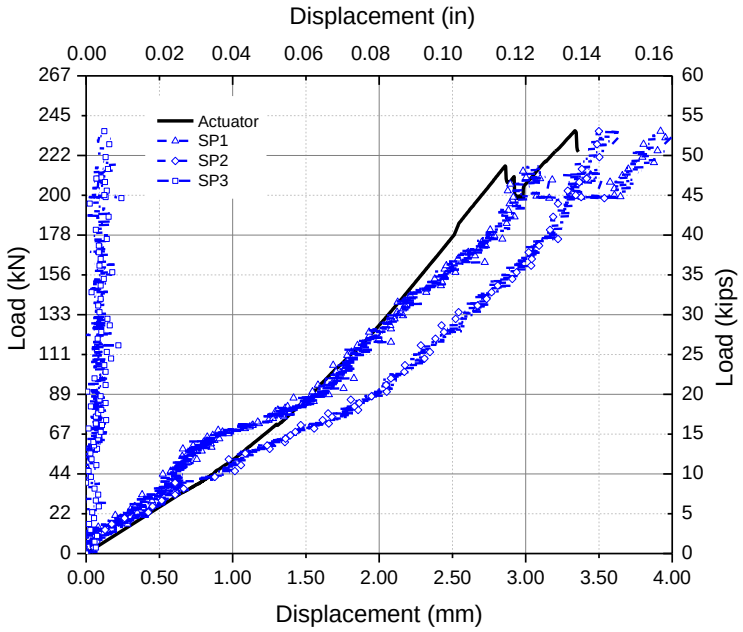

(b) strain-deformation

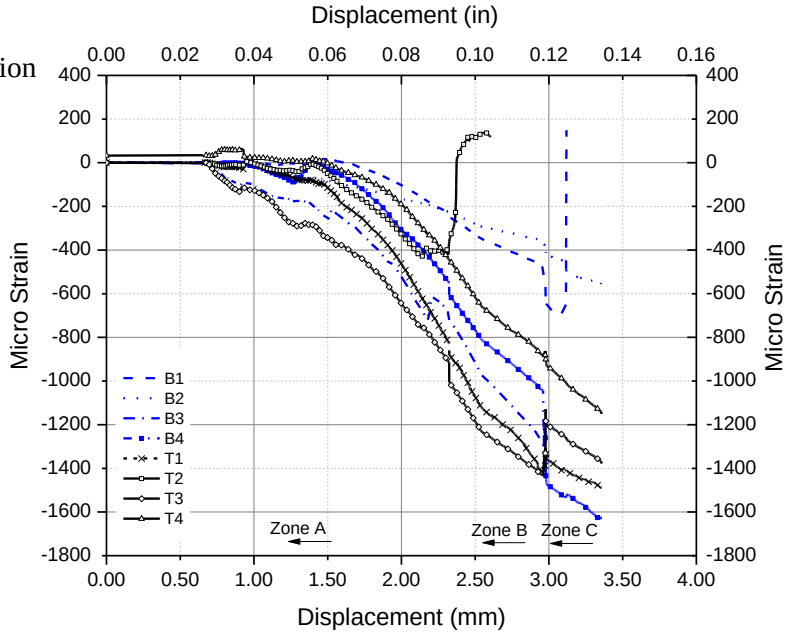

Figure 5: Test outputs; (a) load-deformation, (b) strain in designated members vs. total specimen deformation

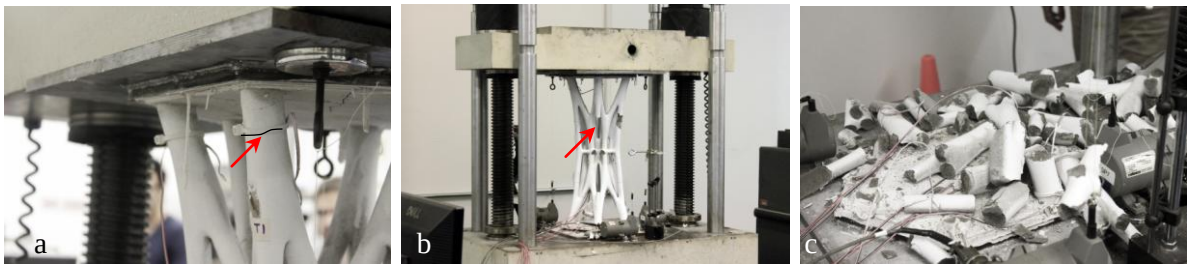

Figure 6: Crack pattern: (a) horizontal crack, (b) failed member, (c) broken specimen

Figure 7 shows the different stages of specimen failure. As it can be seen from Fig.7b, one of the members is popping out by reaching to its maximum buckling load causing the local failure. The specimen failed suddenly in a simultaneous explosive collapse of all core members under its maximum load, see Fig. 7c.

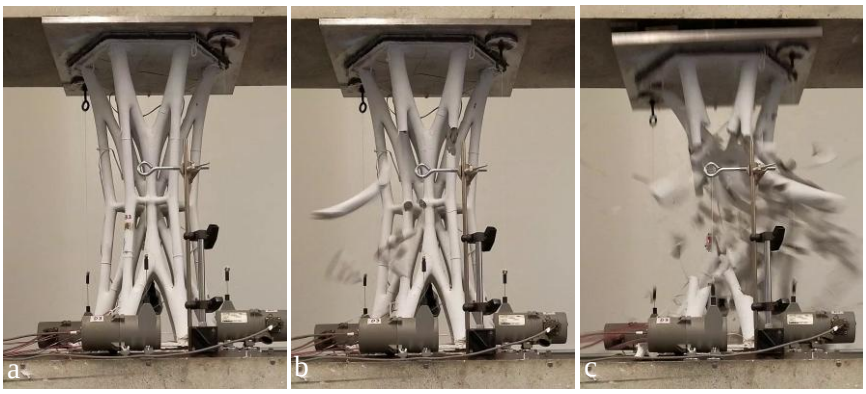

Figure 7: Failure procedure of the specimen: (a) pristine, (b) local buckling, (c) simultaneous collapse

5. Experimental Validation

In the design process external loads at each support is considered as a unit load. Due to the external loads, the force in each member is calculated and sizing of members was associated with the amount of those internal forces. For validating the amount of internal forces in the 3DGS design process, the ultimate load carried by the specimen in the test can be used. Clearly, this is possible only for those members that already have strain gages and experimental forces will be compared with the theoretical ones from 3DGS. Although the ultimate load is 236kN (53.11kips), first peak (216kN (48.69kips)) is chosen here for the comparison between the test results and the model. This is mainly due to uniform load distribution between the members at the first peak. Therefore, external loads on each support in the model is changed to 36kN (216kN/6legs) and internal forces due to these loads are collected from the model and are shown in the Fig. 8.

Internal forces in the test are also calculated through the below procedure:

-Strains of the designated members at the first peak are collected.

-Stresses are calculated using Hook's law ($\sigma_i = E\varepsilon_i$).

-Finally, forces are the product of stress and area of the designated members ($F_i = \sigma_i . A_i$).

The aforementioned process has been done for the B3, B4, T3 and T4 members and final results are presented in the Table 2.

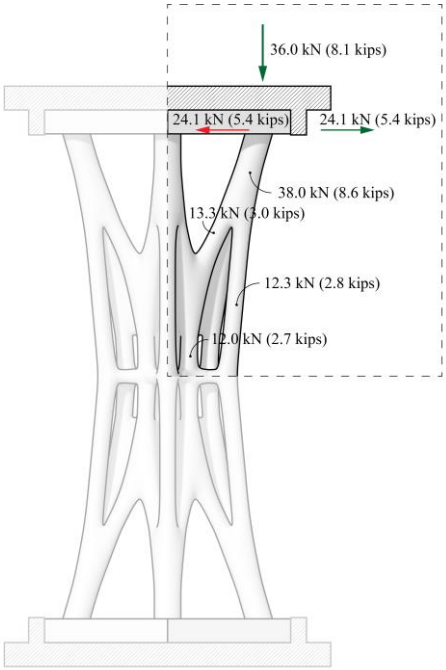

Figure 8: Internal force outputs using 3DGS

Table 2: Internal force calculation using experimental data collected from strain gages

	3DGS kN (kips)	Principal Strain	E GPa (ksi)	Stress MPa (ksi)	Dia. mm (in)	Area mm^2 (in^2)	Force kN (kips)	Error (%)
B3	12.3 (2.7)	0.00140	29.34 (4,256)	41.1 (5.9)	19 (0.75)	2.84 (0.44)	11.7 (2.6)	4.69
B4	12.0 (2.7)	0.00137		40.2 (5.8)			11.5 (2.5)	4.73
T3	12.3 (2.7)	0.00140	29.34 (4,256)	41.1 (5.9)	19 (0.75)	2.84 (0.44)	11.7 (2.6)	4.69
T4	12.0 (2.7)	0.00098		28.9 (4.1)			8.2 (1.8)	31.5

In the members with axial compression force, the experimental results are predicting the load from 3DGS within the 5% error. However, only one of the members (T4) experienced much less strain at the first peak that leads to a lower force compared with 3DGS. For the members with two strain gages first, the principal strain should be calculated and subsequently axial force can be found. This calculation has been done and results are presented in Table 3 for members designated with B1 and B2. As seen from the test results, 3DGS can accurately predict the internal force within the 5% range as actual force. Unfortunately, strain gage T2 failed during the test (refer to Fig. 5b) and force in this member cannot be calculated.

Table 3: Internal force at the support member using strain gages data

	3DGS kN (kips)	Axial Strain	Shear Strain	Principal Strain	E GPa (ksi)	Stress MPa (ksi)	Dia. mm (in)	Area mm^2 (in^2)	Force kN (kips)	Error (%)
B1	38.0 (8.5)	0.00061	0.00023	0.000752	29.3 (4,256)	22.1 (3.2)	46 (1.8)	16.4 (2.54)	36.2 (8.1)	4.58
B2		0.00038								

6. Conclusion

Since material properties are not included in the form finding process, the ultimate strength cannot be predicted in the 3DGS method. Therefore, ultimate strength of the structure should be analytically or experimentally found. For the specimen whose members are sized based on the magnitude of internal forces in 3DGS, the test results show the following; the ratio of the internal force measured in a

member of the specimen over the total applied load in the test is equal to the ratio of the internal force over applied load in 3DGS. That is, the distribution of internal forces measured in test can be accurately predicted by 3DGS. Moreover, the experimental results reveal that local bucking and failure does not immediately cause the global failure of the system due to the indeterminacy of the funicular geometry. The efficiency of spatial funicular system is also verified as all members of the specimen simultaneously collapsed under their maximum strength. Although promising, further studies on the effect of scale and material on the accuracy of force distribution are necessarily in order to assess the final finding of this paper.

Acknowledgment

The authors deeply appreciate the vital contributions of the staff of NDT laboratory at Drexel University who made this project a success.

References

[1] J. C. Maxwell, "On reciprocal figures and diagrams of forces," *Philosophical Magazine,* Series 4, vol. 27 no. 182 pp. 250–261, 1864.

[2] W. J.M. Rankine, *A manual of applied mechanics*, Griffin, London, 1858.

[3] Guastavino/Collins Collection, *Drawings and archives*, Avery Library, Columbia University.

[4] J. Ochsendorf, *Guastavino vaulting, the art of structural tile*, Princeton Architectural Press, New York, 2010.

[5] D. López López, D. Veenendaal, M. Akbarzadeh, P. Block, "Prototype of an ultra-thin, concrete vaulted floor system," *Proceedings of the IASS-SLTE 2014 Symposium, Brasilia, Brazil*, 2014.

[6] A. Liew, D. López López, T. Van Mele, and P. Block, "Design, fabrication and testing of a prototype, thin-vaulted, unreinforced concrete floor," *Engineering Structures*, vol. 137, pp. 323–335, 2017.

[7] M. Akbarzadeh, *3D Graphic Statics Using Polyhedral Reciprocal Diagrams*, PhD thesis, ETHZürich, Zürich, Switzerland, 2016.

[8] M. Bolhassani, M. Akbarzadeh, M. Mahnia and R. Taherian, "On structural behavior of a funicular concrete polyhedral frame designed by 3D graphic statics," *Structures*, vol. 14, pp. 56–68, 2018.

[9] F. Heisel, K. Schlesier, J. Lee, M. Rippmann, N. Saeidi, A. Javadian, D.E. Hebel and P. Block, "Design of a load-bearing mycelium structure through informed structural engineering," *Proceedings of the World Congress on Sustainable Technologies (WCST)*, 2017.

[10] ASTM, C39, *Standard test method for compressive strength of cylindrical concrete specimens*, ASTM International, 2001.

[11] ACI Committee 363, *Report on high-strength concrete (ACI 363R – 10)*, ACI, Farmington Hills, MI, pp. 27.